Chapter 3. Analysis of Simple WAVES Array of Archimedean Spiral Antennas

Stutzman (1983, 1985) presented the concept and theory of a wideband array with variable element sizes (WAVES) in 1983 along with a basic feasibility study. Shively (1988, 1990) extended Stutzman's work and built and measured an eight element planar WAVES array. The WAVES theory, a linear WAVES array, and Shively's planar WAVES array will be reviewed in this chapter. Also, both arrays will be simulated for the first time using the techniques for modeling an Archimedean spiral antenna element presented in the previous chapter.

3.1 Theory of WAVES Array Geometry

The basic geometry of a WAVES array is shown in Fig. 3.1. The larger antenna

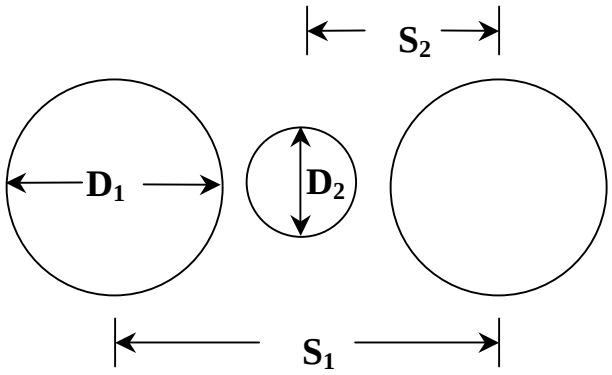

Figure 3.1 Basic Geometry of WAVES Array.

elements are used to cover the first octave of bandwidth. When the grating lobe appears at higher frequencies the smaller antenna is switched on and all three elements are used to cover the next octave of bandwidth. Typically, it is desirable for the inter-element spacing to be between 0.5λ and λ. This leads to a larger element spacing of

$$S_1 = \lambda_1 / 2, \tag{3.1}$$

where λ_1 is the low frequency cutoff for the larger element. From Fig. 3.1, the larger spacing is also given by

$$S_1 = 2S_2 > D_1 + D_2 \tag{3.2}$$

and

$$D_1 = 2D_2, \tag{3.3}$$

where S_2 is the spacing between a larger and smaller element and the diameters of the larger and smaller elements are given by D_1 and D_2, respectively. Combining (3.1), (3.2), and (3.3) the array geometry is given by (Shively, 1988)

$$\begin{aligned} D_1 &= \lambda_1 / 3 \\ D_2 &= D_1 / 2 \\ S_1 &\geq 1.5 D_1 \\ S_2 &= S_1 / 2 \end{aligned} \tag{3.4}$$

Since the larger element is required to cover a minimum of two octaves of bandwidth and it's diameter is required to scale proportionally with frequency an Archimedean spiral antenna was chosen for the WAVES array.

3.2 Two-Octave Linear Array

For simplicity, consider the 3-element WAVES array of Archimedean spirals shown in Fig. 3.2. The low frequency cutoff for the larger element was chosen to be 1000 MHz, which corresponds to a diameter of $D_1 = \lambda_1 / 3 = 0.1m$. Correspondingly, the parameters of the larger elements are $r_2 = 0.05m$ and $N = 16$ and the smaller element is

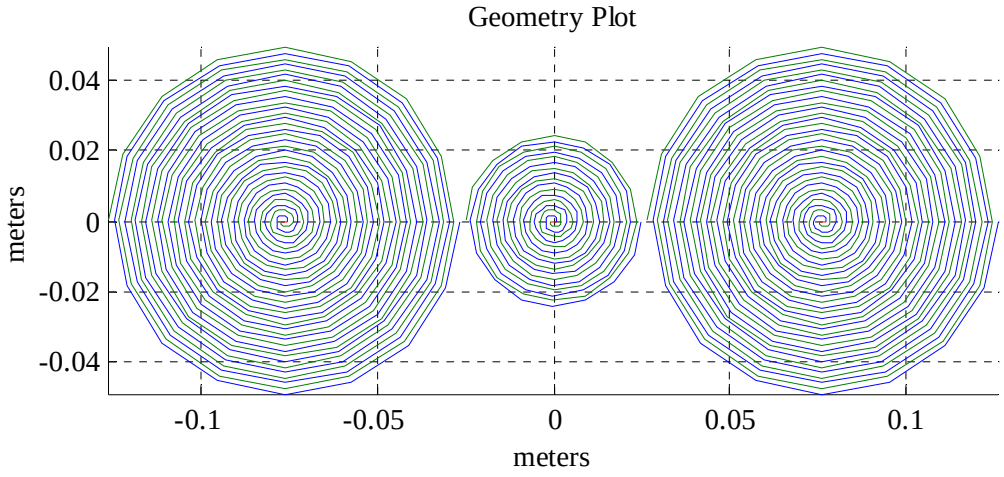

Figure 3.2 Geometry for two octave linear WAVES array.

given by $r_2 = 0.025m$ and $N = 8$. The spacing between the larger elements is given by $S_1 = D_1 + D_2 + 4w = 0.15304m$, where $w = 0.00076m$ is the equivalent strip width of both the larger and smaller spiral. The inter-element spacing was chosen such that the separation between each element in the array is equal to the spacing between each turn of the spiral.

For comparison, the simulation results for the linear array of Fig. 3.2 will be compared to simple array theory. From Stutzman (1998), the normalized array factor for a uniformly excited and equally spaced linear array centered about the origin and oriented along the z-axis is given by

$$f(\psi) = \frac{\sin(N_E \psi / 2)}{N_E \sin(\psi / 2)} \tag{3.5}$$

where N_E is the number of elements in the array. The argument, ψ, is given by

$$\psi = \alpha + \beta d \cos\theta \tag{3.6}$$

where α is the phase taper, $\beta = 2\pi / \lambda$, and d is the element spacing. Following the WAVES concept of switching the higher octave elements on and off as needed, (3.5) reduces to

$$f(\theta) = \cos[(\pi / \lambda) 0.15304 \sin\theta] \tag{3.7}$$

when only the two larger elements are active and

$$f(\theta) = \frac{\sin[(3\pi / \lambda) 0.07652 \sin\theta]}{3\sin[(\pi / \lambda) 0.07652 \sin\theta]} \tag{3.8}$$

when all three elements are active. The phase taper is zero for both cases, $\alpha = 0$, and (3.7) and (3.8) have been modified for an array along the x-axis.

The element pattern must be determined before the simulation results can be compared to the theoretical results. The element pattern is approximated by $g(\theta) = \cos^q(\theta)$. The parameter, q, is found by matching $g(\theta)$ to the simulated element patterns at the chosen angle, θ. The larger element is $6.68dB$ down and the smaller element is $5.32dB$ down at an angle of $\theta = 70°$. Using a 2:1 weighted average in favor of the larger element, since there are two larger elements, q is found by matching $g(\theta)$ to $-6.23dB$ at $\theta = 70°$, giving

$$q = \frac{-6.23}{20\log(\cos 70°)} \tag{3.9}$$

Both element patterns and the corresponding theoretical pattern, $g(\theta) = \cos^{0.669}(\theta)$, are plotted in Fig. 3.3. The simulated patterns and the theoretical pattern match very well for $\pm 70°$ from boresight, but the theoretical pattern has much deeper nulls at broadside.

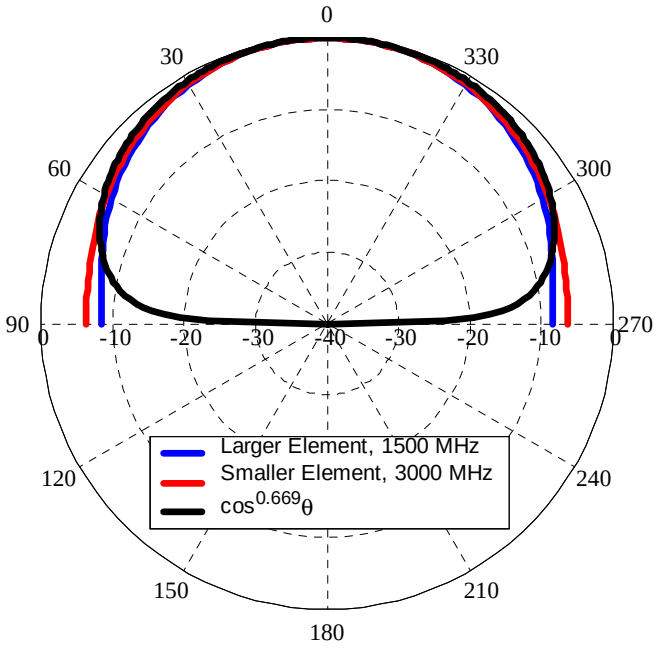

Figure 3.3 Larger and smaller element power pattern for spirals shown in Fig. 3.2 and the corresponding theoretical pattern, $g(\theta) = \cos^{0.669}(\theta)$.

The total theoretical array pattern is found using pattern multiplication giving

$$F(\theta) = g(\theta) f(\theta) \tag{3.10}$$

For the linear array example shown in Fig. 3.2 using (3.7) and (3.8), (3.10) becomes

$$F(\theta) = \cos^{0.669}\theta \cos[(\pi/\lambda)0.15304\sin\theta],\ 1000MHz \le f < 2000MHz \tag{3.11}$$

and

$$F(\theta) = \cos^{0.669}\theta \frac{\sin[(3\pi/\lambda)0.07652\sin\theta]}{3\sin[(\pi/\lambda)0.07652\sin\theta]},\ 2000MHz \le f < 4000MHz \tag{3.12}$$

The theoretical input impedance of the Archimedean spiral is 188Ω. The low frequency and high frequency impedance cutoffs are found by setting the outer and inner circumferences of the spiral equal to one wavelength, respectively. The larger spiral

theoretically operates from $955MHz$ to $62.8GHz$ and the smaller spiral from $1910MHz$ to $62.8GHz$. However, the array pattern performance breaks down above $4000MHz$ due to the appearance of grating lobes so the high frequency impedance cutoff doesn't really affect the array performance. Fig 3.4(a) shows the simulated VSWR of both larger elements for the 3-element linear WAVES array. Only the two larger elements are active and, as expected, both larger elements have identical performance. The low frequency cutoff is approximately 1015 MHz, which is 6.3% above the frequency predicted by theory. The VSWR for a larger and smaller element when all three elements are active is shown in Fig. 3.4(b). Spikes appear in the VSWR of the larger spiral when the smaller element is excited. The low frequency cutoff of the smaller element is about 2275 MHz or 13.8% above the theoretical value.

The radiation patterns for the array are shown in Fig. 3.5. Both simulated and theoretical patterns are plotted. The simulated and theoretical patterns compare very favorably as expected. The major point of interest is the two different plots for a frequency of 2000 MHz, which is the break point between the two octaves. These two plots clearly show the basic principal behind the WAVES theory. Switching on the smaller element eliminates the grating lobe at 2000 MHz and good pattern performance is achieved until about 4000 MHz where the next grating lobe begins to appear.

The gain of the linear array is plotted in Fig. 3.6. The theoretical gain curve was computed using

$$G \approx D = \frac{4\pi}{\Omega_A} \tag{3.13}$$

where

$$\Omega_A = \iint \left| F(\theta) \right|^2 d\Omega \tag{3.14}$$

and $F(\theta)$ is given in (3.11) and (3.12) depending on frequency. The theoretical gain curve shows a jump in the gain where the smaller spiral is switched on and the array goes from 2 to 3 elements. The simulated gain curve is approximately 3 dB lower than predicted by theory over most of the two octaves. At the low end of the frequency range, the simulated gain increases as frequency decreases, which is not intuitive. However, the same trend was seen in Chapter 2 for a single Archimedean spiral antenna and is probably due to the numerical modeling.

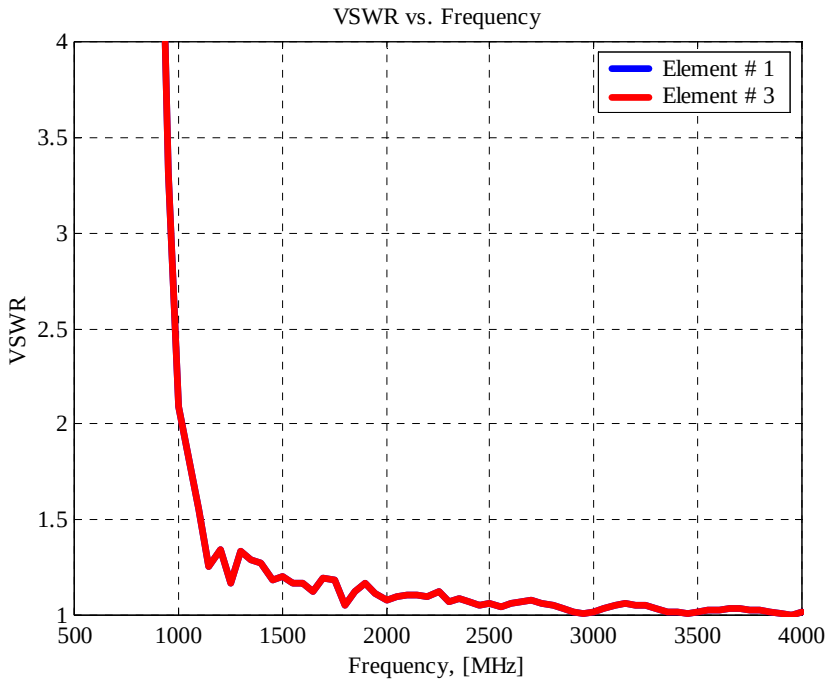

(a) Only larger elements active.

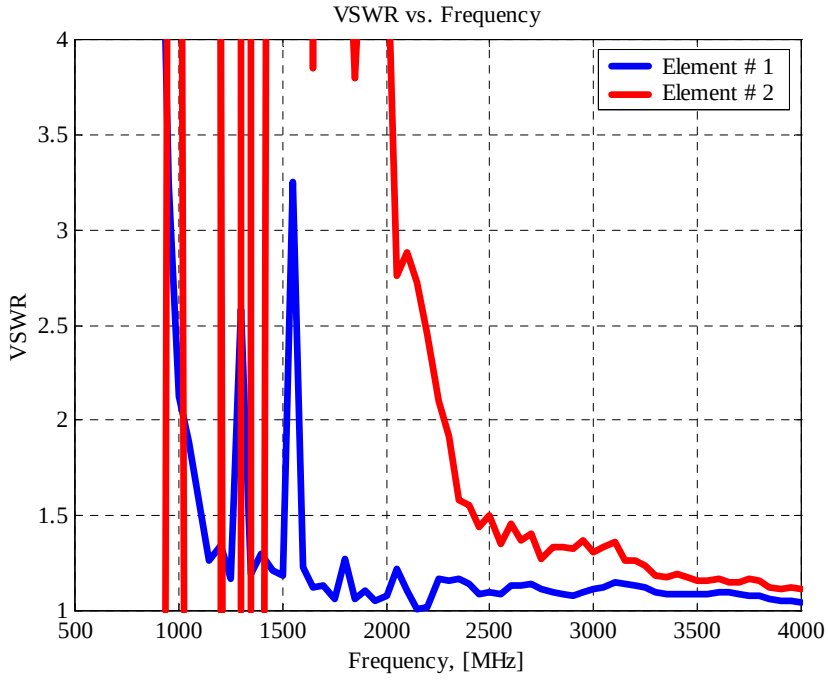

(b) All elements active.

Figure 3.4 Simulated VSWR for 3-element linear WAVES array of Fig 3.2.

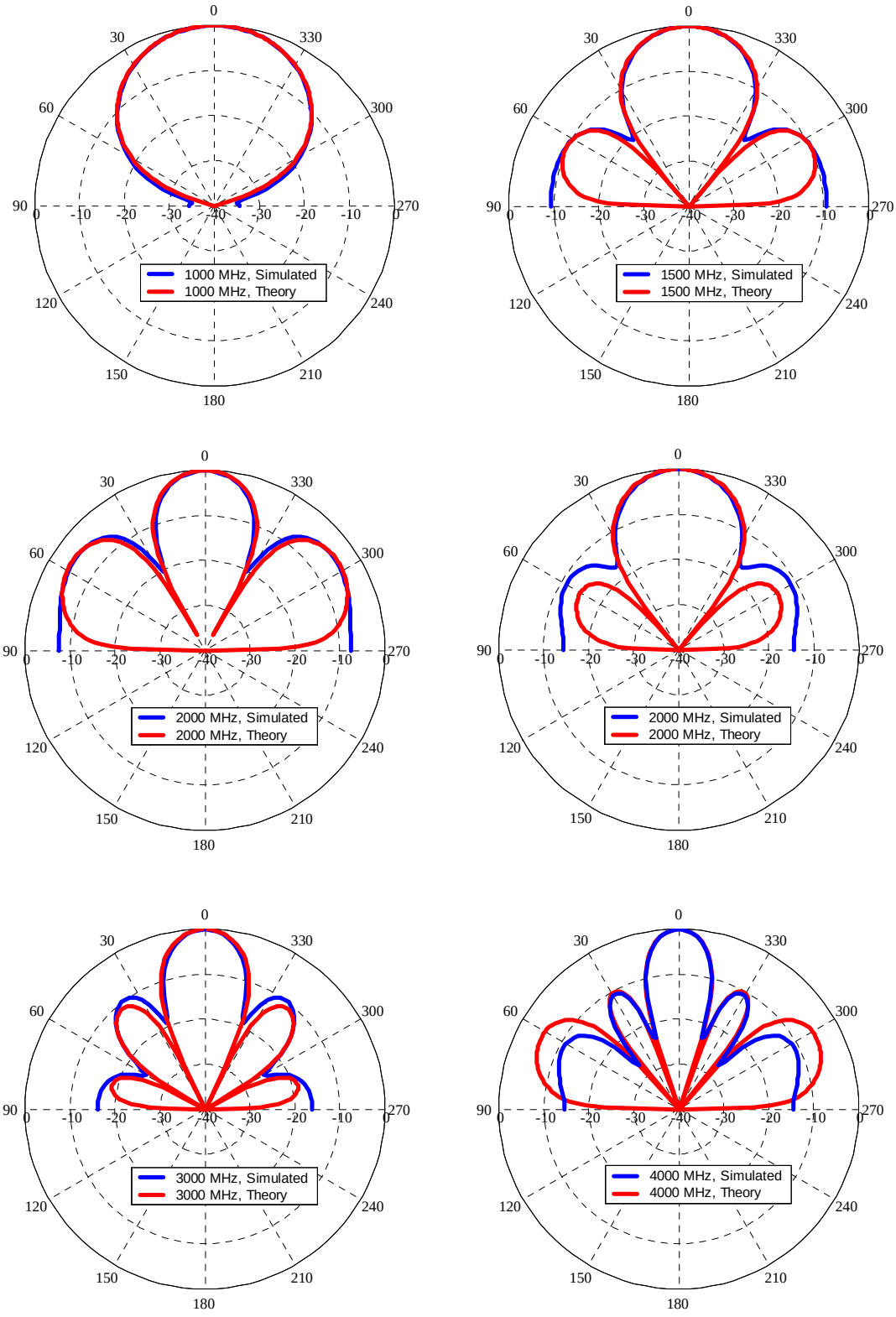

Figure 3.5 Radiation patterns for 3-element linear WAVES array of Fig. 3.2.

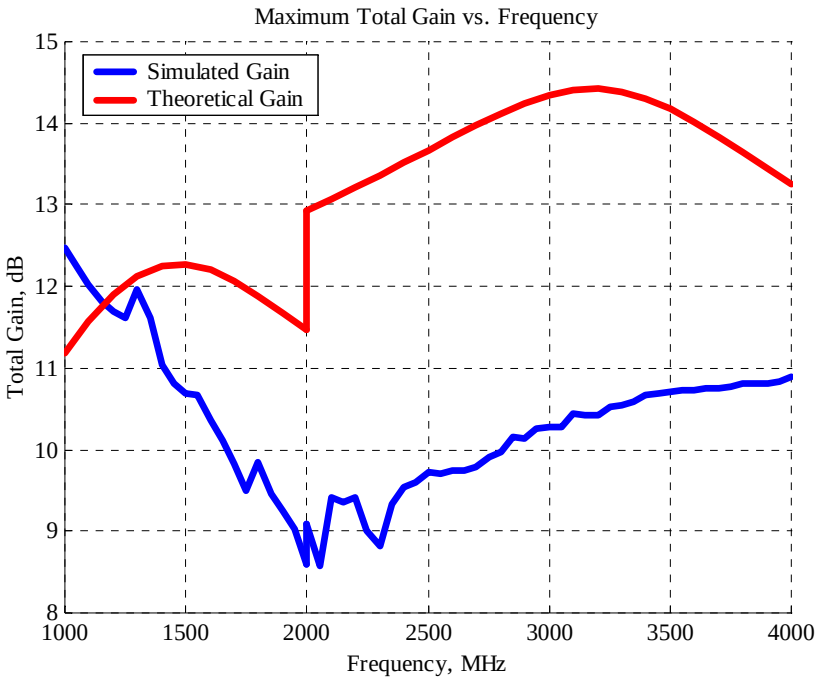

Figure 3.6 Gain curves for the 3-element linear WAVES array of Fig 3.2.

The concept and validity of the WAVES theory has been clearly demonstrated by the simple 3-element linear array example. However, in practice the spirals operate above theoretical low frequency cutoffs due to reflections from the end of each arm of the spiral. This creates a gap in the performance of the array. For the example shown above, there is a gap between 1960 MHz, where the grating lobe due to the two larger elements forms, and 2275 MHz, where the VSWR for the smaller element goes below 2 and can be activated.

One way to possibly solve this problem is to add loss to the spiral to try and minimize the reflections, as demonstrated in Chap. 2. This introduces a new problem of reduced gain. Another solution is to use a planar array as will be shown in the next section. Pattern cuts along the diagonal of a planar array have an effectively closer element spacing that delays the formation of a grating lobe. It may be possible to contain the grating lobe until the VSWR for the smaller element becomes acceptable. However, the problem still exists along the principal axes of the planar array. A third solution is to use a slow-wave spiral to reduce the low frequency cutoff of the spiral. This approach will be pursued in detail in later chapters of this dissertation.

3.3 Two-Octave Planar Array

An array similar to the 8-element planar array presented by Shively and Stutzman (1990) will be reviewed in this section. The array pattern performance along the principal axes is nearly the same for the linear array described in the previous section. So, the performance gap between the two octaves is still a problem. However, along the diagonals the pattern performance is improved due to an effectively closer inter-element spacing and a 1:2:1 amplitude taper for the first octave and a 1:2:2:2:1 amplitude taper for the second octave where all of the elements are active. The 8-element planar WAVES array is shown in Fig. 3.7.

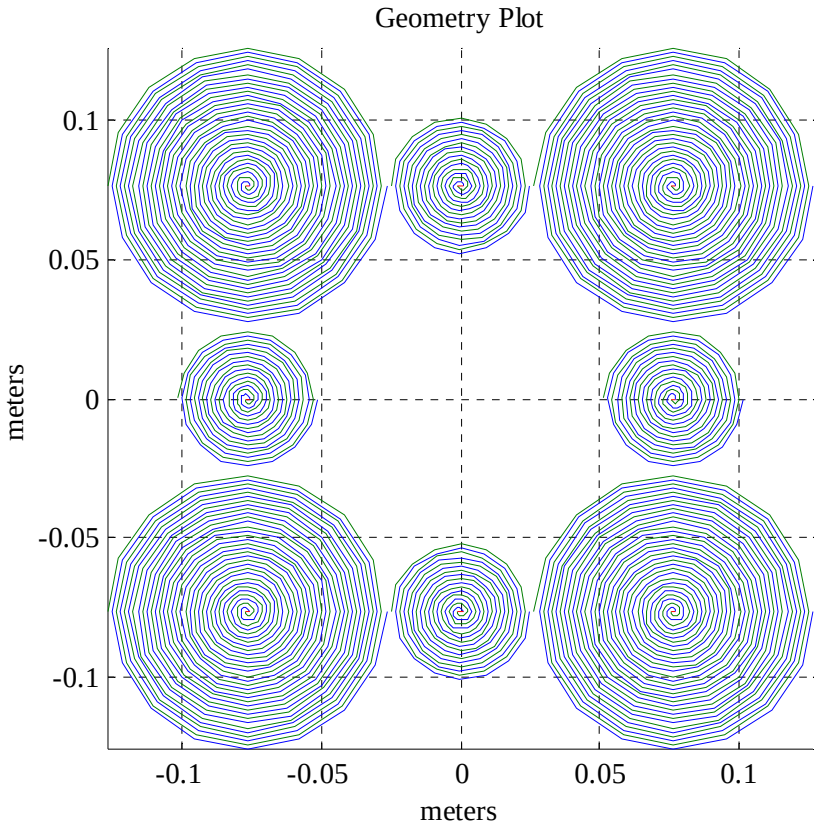

Figure 3.7 Geometry of 8-element planar WAVES array.

The VSWR for the planar array is shown in Fig. 3.8. When only the larger elements are active, Fig. 3.8(a), the VSWR for all 4 elements is basically the same. Compared to the linear array, there is a small spike in the VSWR at 1300 MHz for the

planar array. The low frequency cutoff is 975 MHz, which is 40 MHz lower than the low frequency cutoff observed in the linear array. Fig. 3.8(b) shows the VSWR performance

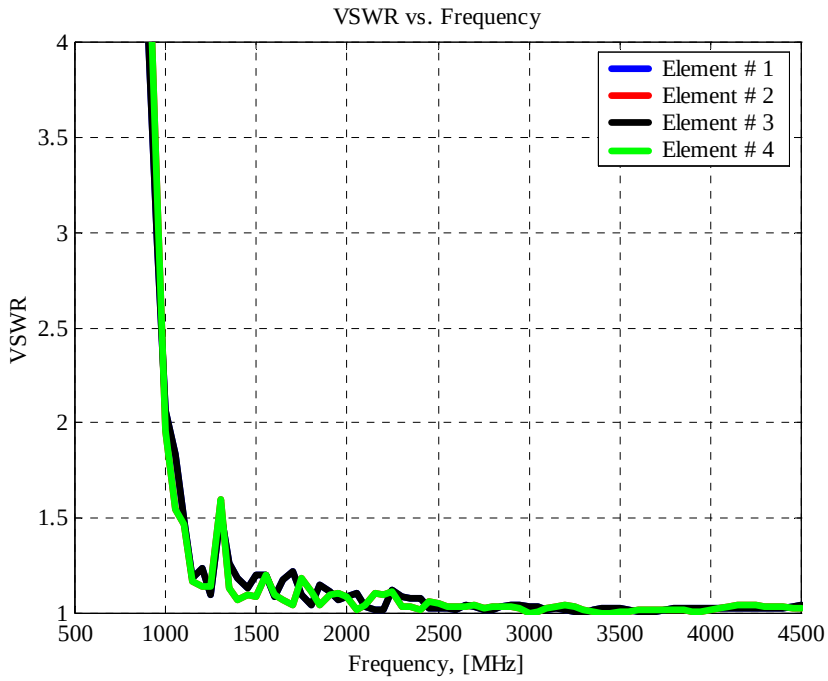

(a) Only 4 larger elements active.

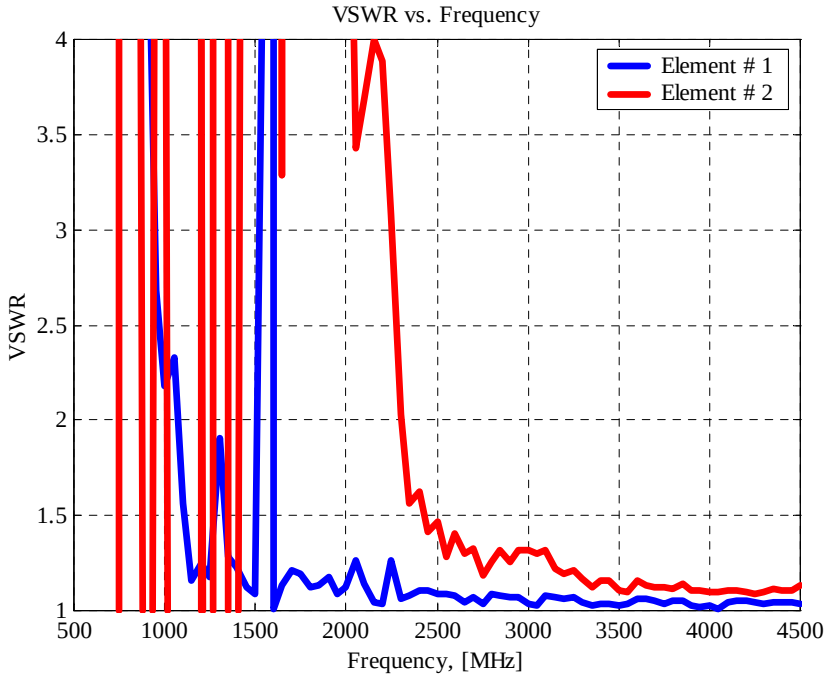

(b) All 8 elements active.

Figure 3.8 VSWR for 8-element planar WAVES array of Fig 3.7.

for the planar array when all elements are active. For purposes of the simulation, an inactive spiral does not have a source, but the feed wire is still included in the model. The figure shows a curve for one larger and one smaller element. The low frequency cutoff for the smaller element is 2300 MHz or 25 MHz higher than for the smaller element in the linear array example. Also, note that the VSWR performance of the larger spirals is greatly decreased below 1700 MHz when all elements are active. This is not a problem if the elements are switched on and off as needed, but the feasibility of leaving all of the elements active at all times for simplicity of operation will be examined in Chapter 6. For that case, the performance of the larger spirals is represented by the blue curve in Fig. 3.8(b).

The mutual coupling in the planar array had opposite effects on the two differently sized spirals. Along the principal axes, the increase in the low frequency cutoff for the smaller elements also increased the performance gap between the two octaves observed in the linear array case. The radiation patterns for the planar array along the principal axes are shown in Fig. 3.9 for completeness. The patterns are nearly identical in both planes and to the linear array example as expected. The smaller elements were switched on at 2000 MHz.

The theoretical patterns for the diagonal or $\phi = 45°$ plane can be found in two ways. A uniformly excited planar array formulation can be used or the equivalent non-uniformly excited, equally spaced, linear array theory may be used. Using the latter, the normalized array factor is (Stutzman and Thiele, 1998)

$$f(\theta) = \frac{\sum_{n=0}^{N-1} A_n e^{j\alpha_n} e^{i\beta z_n \cos\theta}}{\sum_{n=0}^{N-1} A_n} \tag{3.15}$$

where A_n are the element current amplitudes and z_n is the element spacing. As in the linear array example, (3.15) must be modified for the geometry and orientation shown in Fig. 3.6. For the first octave, where only the larger elements are active the inter-element spacing is $d = 0.1082m$ with a 1:2:1 current amplitude. When all elements are active the inter-element spacing is $d = 0.0541m$ with a 1:2:2:2:1 current amplitude. Once again,

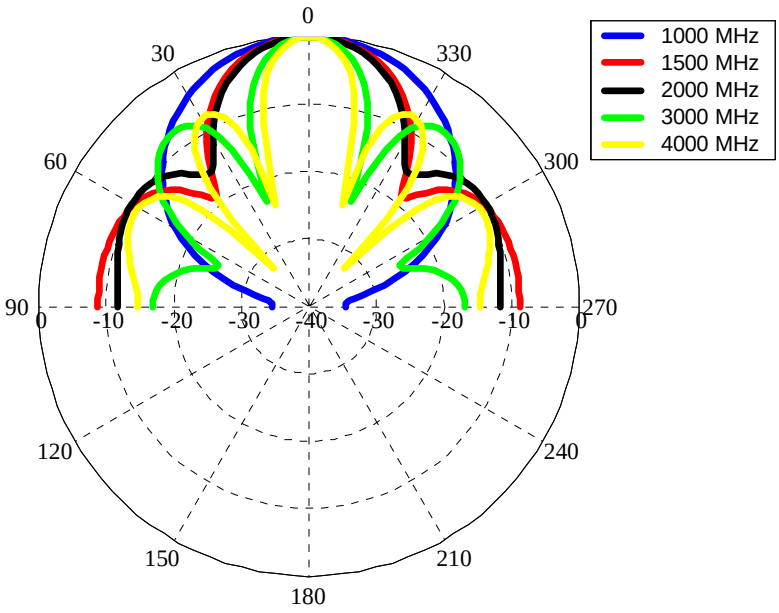

(a) Theta patterns, $\phi = 0°$.

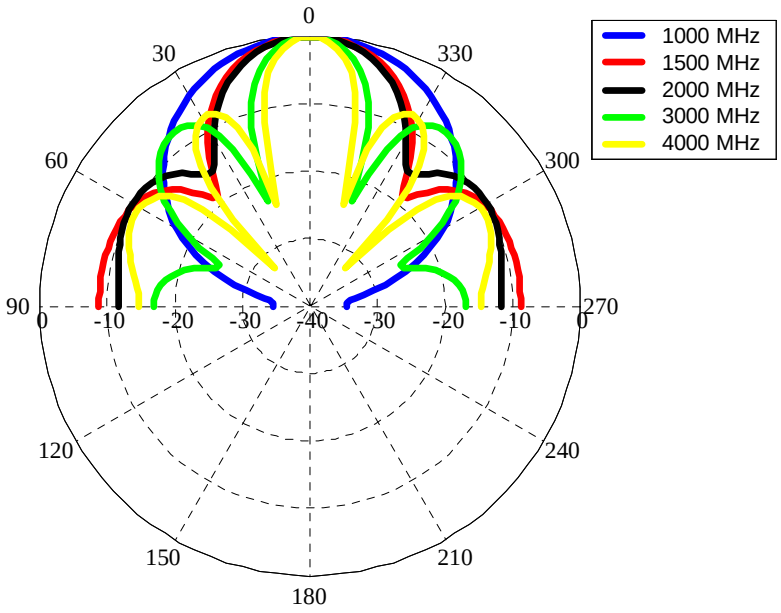

(b) Theta patterns, $\phi = 90°$.

Figure 3.9 Radiation patterns for 8-element planar WAVES array of Fig 3.7. The smaller elements are switched on at 2000 MHz.

the element pattern will be represented by $g(\theta) = \cos^{0.669}(\theta)$. The complete theoretical patterns are given by

$$F(\theta) = \cos^{0.669}(\theta) \frac{\sum_{n=0}^{2} A_n e^{j(2\pi/\lambda)0.1082 n \sin\theta}}{\sum_{n=0}^{2} A_n}, \; 1000MHz \le f \le 2770MHz \qquad (3.16)$$

and

$$F(\theta) = \cos^{0.669}(\theta) \frac{\sum_{n=0}^{4} A_n e^{j(2\pi/\lambda)0.0541 n \sin\theta}}{\sum_{n=0}^{4} A_n}, \; 2770MHz \le f \le 5540MHz \qquad (3.17)$$

The simulated and theoretical patterns are plotted in Fig 3.10 and the gain is shown in Fig. 3.11. Once again the simulated gain is closer to the theoretical results for the second octave. The smaller elements are switched on at 2770 MHz, rather than 2000 MHz as used in the principal planes because of the smaller effective inter-element spacing in the diagonal plane. When the planar array is operated along the diagonal planes the performance of the WAVES array is very good. Both VSWR and radiation patterns are acceptable over a 5.5:1 frequency range. The problem arises if the array is operated in the principal planes. The performance gap in the principal planes will be addressed by the use of slow-wave spiral techniques in Chapter 4.

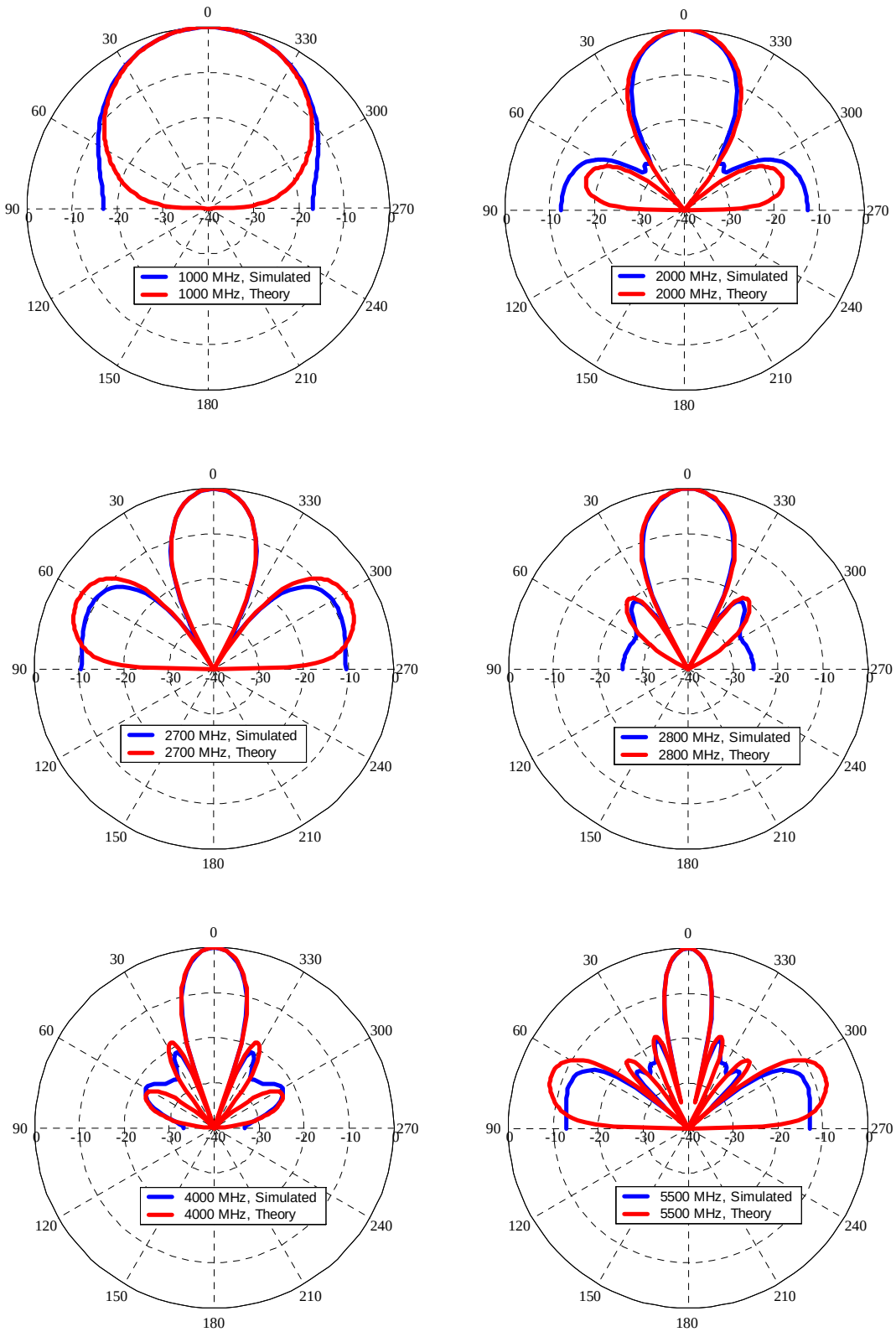

Figure 3.10 Radiation patterns for 8-element planar WAVES array of Fig. 3.7, $\phi = 45°$.

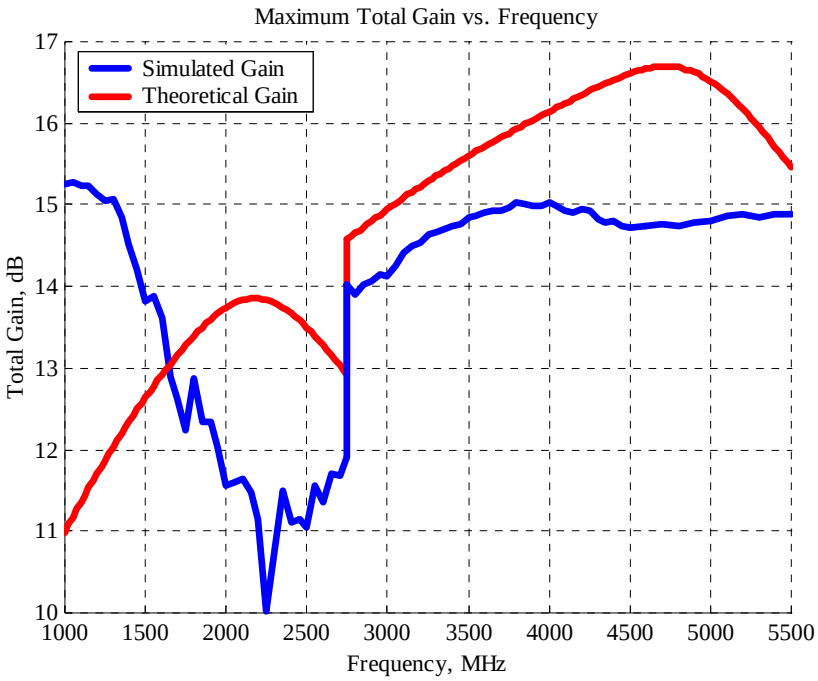

Figure 3.11 Gain of 8-element planar WAVES array of Fig 3.7, $\phi = 45°$.

3.4 Summary

The theory of a wideband array with variable element sizes (WAVES) was presented in this chapter. The early work on WAVES done by Stutzman and Shively was based on simple array theory and measurements. This chapter presented the first full simulation of a three-element, linear WAVES array. The simulation showed a gap in coverage between where the lower octave grating lobe appears and the VSWR for the higher octave becomes better than 2:1. Shively and Stutzman presented measurements of an eight-element planar WAVES array that worked over a two-octave frequency range. The planar array was operated along the diagonals to take advantage of the closer inter-element spacing and inherent amplitude taper, which helped to suppress the grating lobes. Simulations of this eight-element planar array were also performed. The array worked well along the diagonals but still had a performance gap along the principal planes. The following chapter will outline the performance of a new spiral element called the star spiral. It will be shown in later chapters that the star spiral can be used to eliminate the

performance gap observed in this chapter for a linear WAVES array of Archimedean spirals.